Article

Facile Fabrication of Absorption-Dominated Biodegradable Poly(lactic acid)/Polycaprolactone/Multi-Walled Carbon Nanotube Foams towards Electromagnetic Interference Shielding

Tong Liu [1,2], Huiyao Feng [2], Weiqiang Zeng [2], Chenhong Jin [2] and Tairong Kuang [2,*]

[1] Department of Polymer Science and Engineering, Zhejiang University, Hangzhou 310027, China; liut@zjut.edu.cn

[2] Zhejiang Key Laboratory of Plastic Modification and Processing Technology, College of Material Science and Engineering, Zhejiang University of Technology, Hangzhou 310014, China; fenghhyyy@163.com (H.F.); zengweiqiang06@163.com (W.Z.); 19817479399@163.com (C.J.)

[*] Correspondence: kuangtr@zjut.edu.cn

Abstract: The use of electromagnetic interference shielding materials in the mitigation of electromagnetic pollution requires a broader perspective, encompassing not only the enhancement of the overall shielding efficiency (SE_T), but also the distinct emphasis on the contribution of the absorption shielding efficiency within the total shielding efficiency (SE_A/SE_T). The development of lightweight, biodegradable electromagnetic interference shielding materials with dominant absorption mechanisms is of paramount importance in reducing electromagnetic pollution and the environmental impact. This study presents a successful fabrication strategy for a poly(lactic acid)/polycaprolactone/multi-walled carbon nanotube (PCL/PLA/MWCNT) composite foam, featuring a uniform porous structure. In this approach, melt mixing is combined with particle leaching techniques to create a co-continuous phase morphology when PCL and PLA are present in equal mass ratios. The MWCNT is selectively dispersed within the PCL matrix, which facilitates the formation of a robust conductive network within this morphology. In addition, the addition of the MWCNT content reduces the size of the phase domain in the PCL/PLA/MWCNT composite, showing an adept ability to construct a compact and stable conductive network. Based on its porous architecture and continuous conductive network, the composite foam with an 80% porosity and 7 wt% MWCNT content manifests an exceptional EMI shielding performance. The SE_T, specific SE_T, and SE_A/SE_T values achieved are 22.88 dB, 88.68 dB·cm³/g, and 85.80%, respectively. Additionally, the resulting composite foams exhibit a certain resistance to compression-induced deformations. In summary, this study introduces a practical solution that facilitates the production of absorption-dominated, lightweight, and biodegradable EMI shielding materials at scale.

Keywords: PCL/PLA/MWCNT; composite foams; morphological characteristics; electrical conductivity; EMI shielding

1. Introduction

With the rapid advancement of electronic information technology, a new era of highly integrated and powerful electronic devices has emerged. Consequently, electromagnetic pollution has become a critical issue as a result of the escalating problem. If electromagnetic pollution is not effectively managed via efficient electromagnetic interference shielding materials, it can adversely affect not only the functioning stability of the equipment, its service life, and its efficiency, but it can also have irreversible effects upon human health as well. Unlike metal counterparts, polymer-based EMI shielding materials have garnered considerable interest from both academia and the industry. The allure of these materials

lies in their versatile design capabilities, lightweight nature, cost-effectiveness, and ease of processing [1–4]. Within this domain, the emergence of biodegradable polymer-based EMI shielding materials stands out as prominent contenders due to their intrinsic environmentally benign characteristics [5–7]. In the past few decades, polylactic acid (PLA), polybutylene succinate (PBS), polycaprolactone (PCL), and polybutylene adipate terephthalate (PBAT) have been combined with conductive or magnetic fillers like carbon black (CB), carbon nanotube (CNT), silver nanowire (SNW), MXene, and Fe_3O_4 to fabricate biodegradable polymer EMI shielding materials using techniques such as melt blending, solution mixing, and interface engineering [8–25]. Creating an unbroken and reliable conductive pathway stands as an essential prerequisite for polymer/filler composites to exhibit noteworthy electromagnetic interference (EMI) shielding capabilities. The conventional approach involves incorporating a higher proportion of conductive fillers into the polymer matrix to establish a continuous and stable conductive route. This, however, introduces elevated expenses and processing intricacies. Moreover, the escalating filler content exacerbates challenges in attaining a uniform dispersion within the polymer matrix, resulting in filler agglomerations that subsequently compromise both the EMI shielding efficiency and mechanical characteristics of the final composites. Addressing these concerns, researchers have proposed strategies for selectively dispersing fillers in multi-phase, multi-component systems by modulating interfacial interactions. This approach achieves low-cost, high-utilization filler incorporation and robust mechanical properties [26–30]. For instance, Xu et al. investigated the phase morphology effects on the electrical properties in PLA/PCL/Acid-CNT composites through varying the PLA/PCL ratios [26]. Optimal electrical conductivity was achieved at a 60:40 mass ratio, which was attributed to the selective dispersion of CNT in the PCL component, fostering the formation of a co-continuous structure. Similarly, Chen at al. introduced graphene oxide (GO) to immiscible PLLA/EVA systems, selectively dispersing GO at two-phase interfaces through π-π stacking interactions with CNT [30]. This led to significantly lower percolation thresholds in the PLLA/EV/CNT/GO composites, highlighting the efficacy of selective filler dispersion in reducing filler dosages. As demonstrated above, the selective dispersion of functional fillers in the co-continuous polymer blending system via interfacial engineering can indeed reduce filler dosages.

Central to EMI shielding effectiveness is the composition of the total shielding efficiency (SE_T), encompassing the absorption shielding efficiency (SE_A) and the reflection shielding efficiency (SE_R). A higher proportion of SE_A in SE_T reduces the reflected electromagnetic waves, which can compromise electronics. Thus, the quest for polymer-based EMI shielding materials necessitates a focus on not only augmenting SE_T, but also elevating the SE_A/SE_T ratio, indicating a superior performance. To this end, creating porous structures in shielding materials has proven to be effective, whereby electromagnetic waves undergo repeated reflection, attenuation, and eventual absorption [31]. Several methods, including supercritical fluid foaming [32–35], particle leaching [36–38], phase separation [39–41], and freeze drying [42–44], have been developed for fabricating porous polymer-based shielding materials. Among these, particle leaching employing water-soluble inorganic salt particles as pore-inducing agents holds promise due to its scalability, controllable pore architecture, affordability, and potential for agent recycling.

In this study, we employ PCL and PLA as the biodegradable polymer matrixes and MWCNT as the conductive filler. The resultant PCL/PLA/MWCNT composites, characterized by selectively dispersed fillers, are achieved through traditional melt blending. Subsequently, these composites undergo further melt mixing with NaCl particles, followed by pore-inducing agent removal through water treatment, yielding PCL/PLA/MWCNT composite foams. To evaluate filler dispersion effects on conductivity, EMI shielding, and thermodynamic properties, we comprehensively investigate MWCNT dispersion through scanning electron microscopy (SEM), rheological measurements, differential scanning calorimetry (DSC), and thermogravimetric analysis (TGA). Through a comparative assessment of specific EMI SE_T and SE_A/SE_T values between solid and porous composites,

the advantages of pore structures in fabricating absorption-dominated and biodegradable polymer-based EMI shielding materials are highlighted. This study contributes to the understanding and advancement of lightweight, environmentally benign, and highly effective EMI shielding materials.

2. Experimental Procedure

2.1. Materials

The commercial polycaprolactone (PCL) CAPA 6500, which has an average molecular weight of 5.0×10^4 g/mol, a melting point of 60–65 °C, and a density of 1.02 g/cm^3, was purchased from Perstorp Ltd. (Stenungsund, Sweden). Polylactic acid (PLA) 4032D, supplied by NatureWorks Ltd. (Plymouth, MN, USA), has a weight average molecular weight and density of 2.23×10^5 g/mol and 1.24 g/cm^3. MWCNT Nanocyl^{TM} NC7000 (Nanocyl SA, Sambreville, Belgium) was used in this study, and its average diameter, length, specific surface area, and carbon purity are 10 nm, 1.5 μm, 250–300 m^2/g, and 90%, respectively. NaCl particles (GR) were provided by Sinopharm Group Chemical Reagents Co., Ltd. (Shanghai, China). The glacial acetic acid (AR) used in this study was purchased from Guangdong Guanghua Chemical Factory Co., Ltd. (Guangzhou, China). All raw materials were used without any additional treatment.

2.2. Samples Preparation

Figure 1 illustrates the preparation process of PCL/MWCNT composites, PCL/PLA/MWCNT composites, and PCL/PLA/MWCNT composite foams. Melt blending of PCL and MWCNT (PCL/MWCNT composites) was performed using a torque rheometer (Haake PolyLab QC, Thermo Fisher Scientific Co., Ltd., Shanghai, China) at a processing temperature, rotor speed, and mixing time of 100 °C, 50 rpm, and 5 min, respectively. The MWCNT mass fraction within the PCL/MWCNT composites was varied as follows: 1 wt%, 3 wt%, 5 wt%, and 7 wt%.
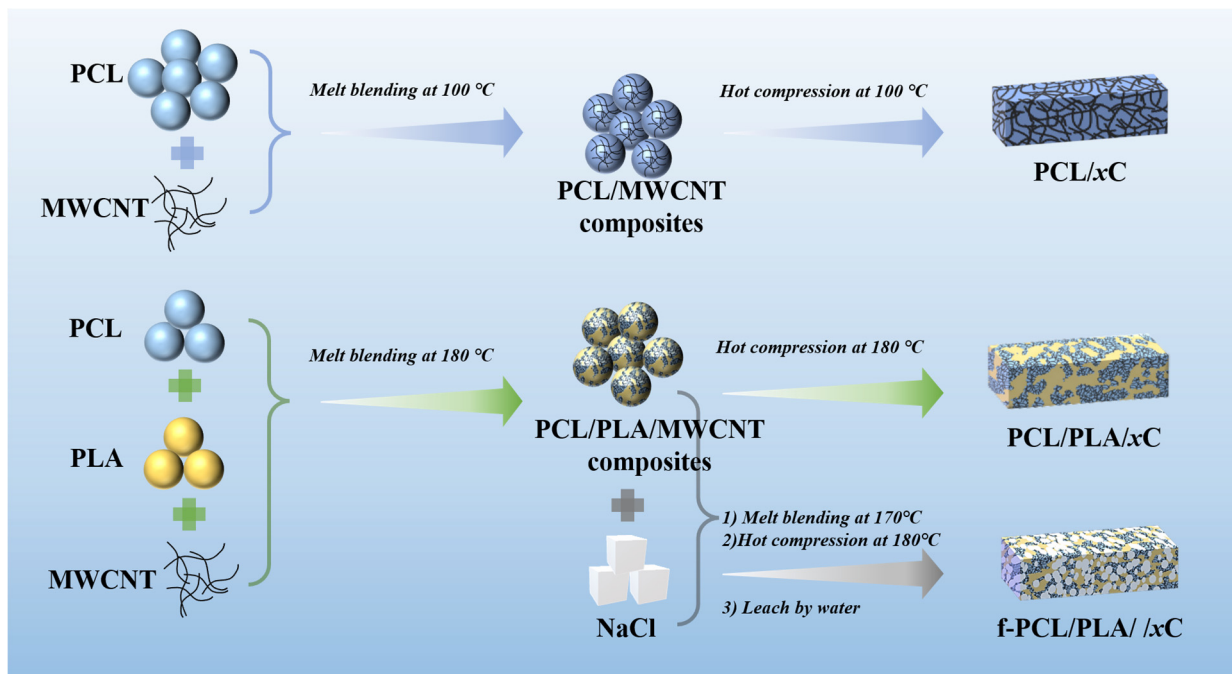

Figure 1. Schematic diagram for the preparation of PCL/*x*C, PCL/PLA/*x*C, and f-PCL/PLA/*x*C samples.

Similarly, PCL/PLA/MWCNT composites were prepared using the same method under a processing temperature of 180 °C, rotor speed of 50 rpm, and mixing time of 5 min. In these composites, the mass fraction of MWCNT was once again varied at 1%, 3%, 5%, and 7%, with PLA and PCL maintained in a balanced mass ratio (50/50).

The prepared PCL/PLA/MWCNT composites were further melt-blended with NaCl particles according to a volume ratio of 80:20 to obtain PCL/PLA/MWCNT/NaCl composites. The processing temperature, rotor speed, and mixing time were 180 °C, 50 rpm, and 5 min, respectively. The resultant PCL/PLA/MWCNT/NaCl composites were subsequently subjected to iterative deionized water washing, effectively eliminating the NaCl content and leading to the formation of the PCL/PLA/MWCNT foam. For the sake of clarity, the following designations were used throughout this study: PCL/xC for PCL/MWCNT composites; PCL/PLA/xC for PCL/PLA/MWCNT composites; and f-PCL/PLA/xC for composite foams containing PCL/PLA/MWCNT, with x indicating the mass percentage of MWCNT.

2.3. Methods of Characterization

Scanning Electron Microscopy (SEM). The cryo-fractured surface morphologies of PCL/xC, PCL/PLA/xC, and f-PCL/PLA/xC samples were observed using a HITACHI Regulus 8100 scanning electron microscope (SEM, Hitachi Scientific Instruments Co., Ltd., Beijing, China). To investigate the distribution of MWCNT in PCL/PLA/xC composites and the phase morphology evolution with MWCNT content, the cryo-fractured surface of PCL/PLA/xC composites was immersed in glacial acetic acid for 30 min to remove PCL phase. Subsequently, the surface was thoroughly rinsed with deionized water. All samples were completely dried and coated with a layer of gold before SEM observation.

Rheological Measurement. The rheological behavior of PCL/xC and PCL/PLA/xC composites were characterized using a rotational rheometer (MCR302, Anton Paar Instrument Co., Ltd., Shanghai, China) at 100 °C and 180 °C, respectively, employing a dynamic frequency sweep mode. The strain was set at 1%, and the frequency sweep ranged from 1 to 100 rad/s.

Differential Scanning Calorimetry (DSC). DSC experiments were conducted on each sample using a Netzsch DSC 214 (Netzsch Scientific Instrument Trading Co., Ltd., Shanghai, China). For PCL/xC and PCL/PLA/xC composites, approximately 7 mg of samples was subjected to heating from ambient temperature to 120 °C and 200 °C, respectively, at a constant rate of 10 °C/min under a N_2 atmosphere.

Thermogravimetric Analysis (TGA). The thermal stability of PCL/xC and PCL/PLA/xC composites with varying MWCNT contents was assessed using a thermogravimetric analyzer (TGA 209F1, Netzsch Scientific Instrument Trading Co., Ltd., Shanghai, China) under nitrogen protection. Each sample, weighing about 7 mg, was heated from ambient temperature to 600 °C at a constant rate of 10 °C/min.

Mechanical Properties. Compression properties of f-PCL/PLA/xC samples were determined using an Instron 5566 universal mechanical testing instrument (Instron Test Equipment Trading Co., Ltd., Shanghai, China). Testing was conducted at a speed of 5 mm/min, and each sample underwent five tests at room temperature.

Electrical Conductivity. The electrical conductivity of solid and foamed samples was measured using a four-point probe resistivity measurement system (RTS-9, Guangzhou Four Probe Technology Co., Ltd., Guangzhou, China) and a high resistance meter (ZC36, Shanghai Anbiao Electronic Ltd., Shanghai, China).

Electromagnetic interference shielding efficiency (EMI SE). The EMI SE of PCL/xC, PCL/PLA/xC, and f-PCL/PLA/xC samples was quantified using a Ceyear 3672C-S vector network analyzer (Ceyear Technologies Co., Ltd., Qingdao, China) within the X-band frequency range (8.2–12.4 GHz). For measurements, all samples were cut into cuboid shapes with dimensions of 22.86 mm × 10.16 mm × 3.00 mm. EMI SE is defined by the following formula: $SE = 10 \log P_i/P_t$, where P_i and P_t represent the energies of incident and transmitted waves [3,45]. For example, a material with an SE of 20 dB means that 99% of the electromagnetic wave is shielded and only 1% of the energy is filtered through, which meets the commercial standard.

3. Phase Morphology and Crystal Structure

The rheological properties of the PCL/xC composites are presented in Figure 2. As illustrated in Figure 2a, the complex viscosity of the PCL/xC composites increases with the increasing MWCNT content across the tested frequency ranges, demonstrating a notable viscosity-altering impact of MWCNT on the PCL matrix. Furthermore, the complex viscosity of both the PCL and PCL/xC composites decreases with the increasing shear frequency, which is indicative of the shear-thinning non-Newtonian fluids' behavior. With the increasing MWCNT content, the frequency-dependent tendencies of the storage modulus (G′) and loss modulus (G″) gradually weaken (Figure 2b,c). This implies that composites with an increased MWCNT content gradually transition from exhibiting liquid-like rheological characteristics to solid-like behavior, in contrast to the pure PCL matrix. In Figure 2d, the tan δ curve exhibits a downward shift upon the introduction of MWCNT. Additionally, the curve demonstrates a gentler slope as the MWCNT content increases, indicating a reduced frequency dependence of tan δ. This suggests the possible formation of a physical network of MWCNTs, serving as entanglements within the composites.
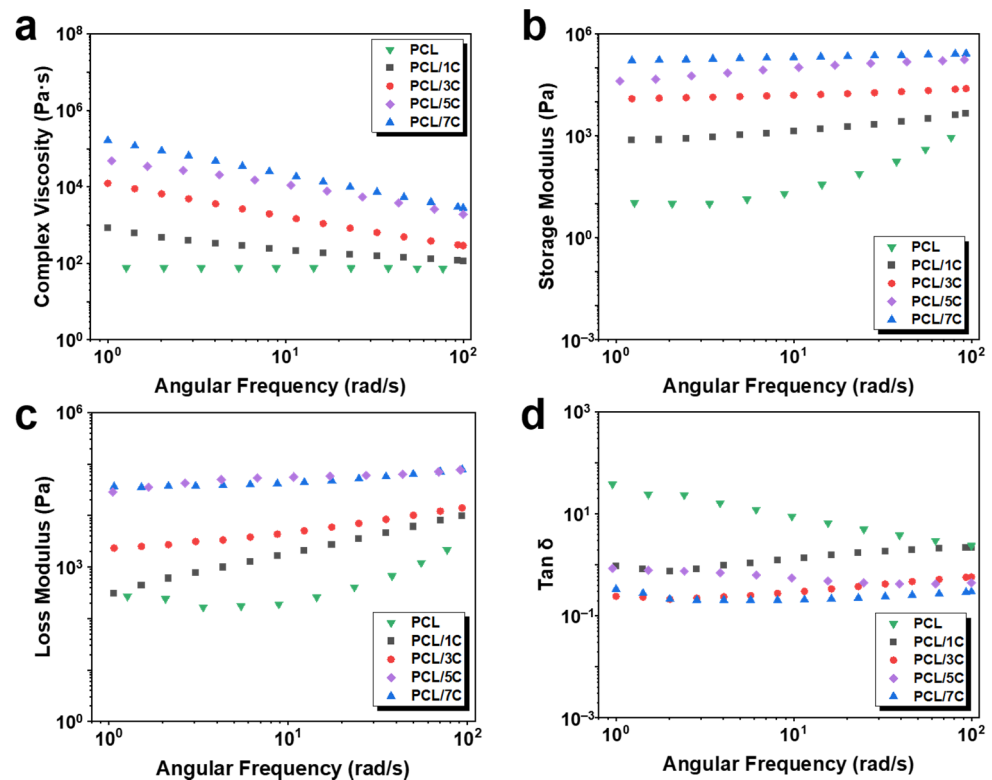

Figure 2. Rheological properties of PCL/xC composites: (**a**) complex viscosity, (**b**) storage modulus, (**c**) loss modulus, and (**d**) tan δ.

The results obtained from the DSC curves reveal that the incorporation of MWCNT induces a marginal elevation in the melting temperature and crystallinity compared to the pure PCL, which is primarily attributed to the heterogeneous nucleation effect (Figure 3a) [46,47]. Conversely, the TGA results (Figure 3b) indicate a slight reduction in the initial thermal decomposition temperature of the PCL/xC composites upon MWCNT addition, and a similar investigation was reported in [48]. This observation might be attributed to the facilitated heat transfer to the interior of the composites due to the established MWCNT network, thereby expediting the thermal decomposition. As expected, the residue mass of the PCL/xC composites progressively escalates with the increased MWCNT content. This phenomenon is predominantly ascribed to the presence of an undecomposed MWCNT filler.
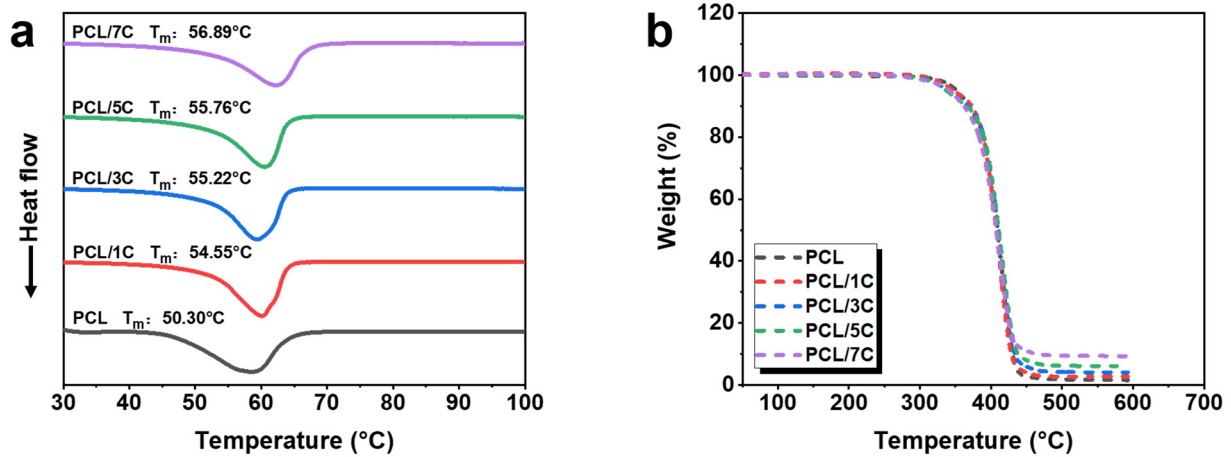
Figure 3. DSC (**a**) and TG (**b**) heating curves of PCL/*x*C composites.

Figure 4 displays the cryo-fractured surface SEM images of the PCL/*x*C composites. In contrast to the smooth morphology exhibited by the pure PCL (as depicted in Figure S1a), discernible MWCNT components are evident within the PCL/*x*C composite (visible as small white bright spots in Figure 4). As is well known, whether a complete and stable conductive network can be constructed will greatly affect the EMI shielding performance. It can be found that MWCNT achieves uniform dispersion in the PCL matrix even when the filler content is as high as 7%, which is conducive to the construction of a completely conductive network.
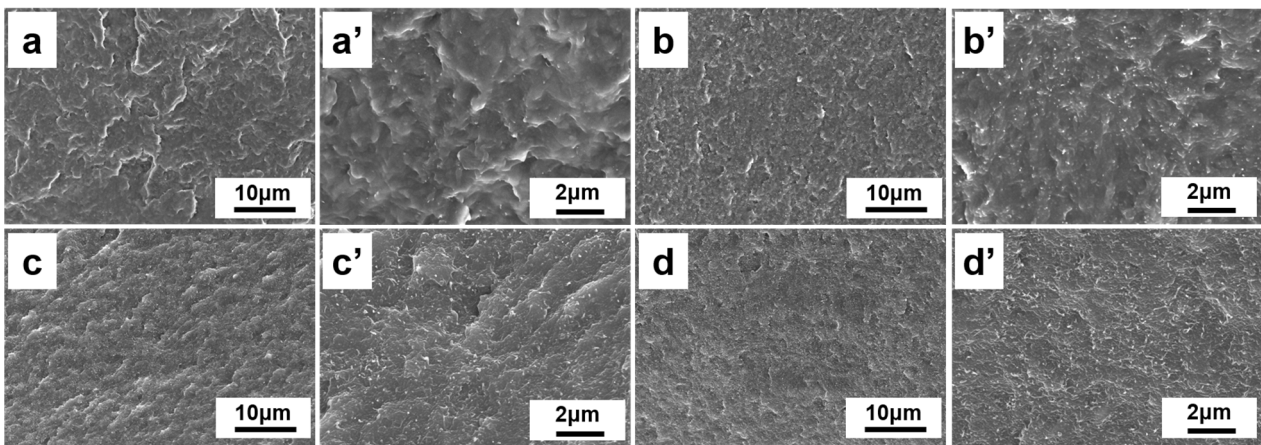

Figure 4. SEM images of cryo-fractured surfaces of PCL/*x*C composites: (**a**,**a'**) PCL/1C, (**b**,**b'**) PCL/3C, (**c**,**c'**) PCL/5C, and (**d**,**d'**) PCL/7C.

Figure 5a shows the electrical conductivity of both the pure PCL and the PCL/*x*C composites. The establishment of a conductive network through MWCNT incorporation results in the electrical conductivity of the PCL/*x*C composites being increased by approximately 11~12 orders of magnitude compared to the pure PCL (Table S1). Notably, for PCL/1C, when the MWCNT content is merely 1 wt%, the electrical conductivity attains 4.12 S/m, representing an increase of about 11 orders of magnitude from the 5.10×10^{-11} S/m exhibited by the pure PCL. However, with a subsequent increase in the MWCNT content, the increase trend in the electrical conductivity of PCL/*x*C composites demonstrates a gradual deceleration. For example, there is a transition from PCL/1C with a 4.12 S/m to PCL/7C with a 142.10 S/m when the MWCNT content is increased from 1 wt% to 7 wt%. The outcomes of the electrical conductivity tests harmoniously corroborate the findings from the SEM and rheological assessments. These results are largely attributed to the good dispersion of MWCNT, facilitating the formation of a relatively complete conductive network

even at low filler loadings. Beyond this point, a further increment in the filler content no longer yields a clearly discernible qualitative effect on the integrity of conductive networks. In accordance with the public reports in the literature, the EMI SE of polymer-based shielding materials exhibits a positive correlation with electrical conductivity [2,3]. Figure 5b,c presents the EMI shielding performance of the PCL/xC composites. The EMI shielding performance across the tested frequency range of all the PCL/xC composites is stable, indicating a uniform distribution of the conductive network. As expected, the total EMI SE of the PCL/xC composites increases with the increasing MWCNT content, as demonstrated by the electrical conductivity test results. Furthermore, as shown in Figure 5c, the SE_A is greater than the SE_R in the composition of the SE_T, demonstrating that the absorption loss is the principal mechanism for EMI shielding. It is noteworthy that despite the good electrical conductivity observed in the PCL/1C composite, its EMI SE_T is modest at only 6.68 dB. This phenomenon is essentially attributed to the propensity of EMW to penetrate through sparsely interconnected conductive networks (lower filler contents), whereas the possibility of EMW escape is significantly reduced within denser networks formed at higher MWCNT contents. Consistently, the EMI SE_T of the PCL/5C and PCL/7C composites surpasses the commercial requirement of 20 dB when the MWCNT content is increased beyond 5 wt%, reaching values of 22.75 dB and 32.07 dB, respectively [49].
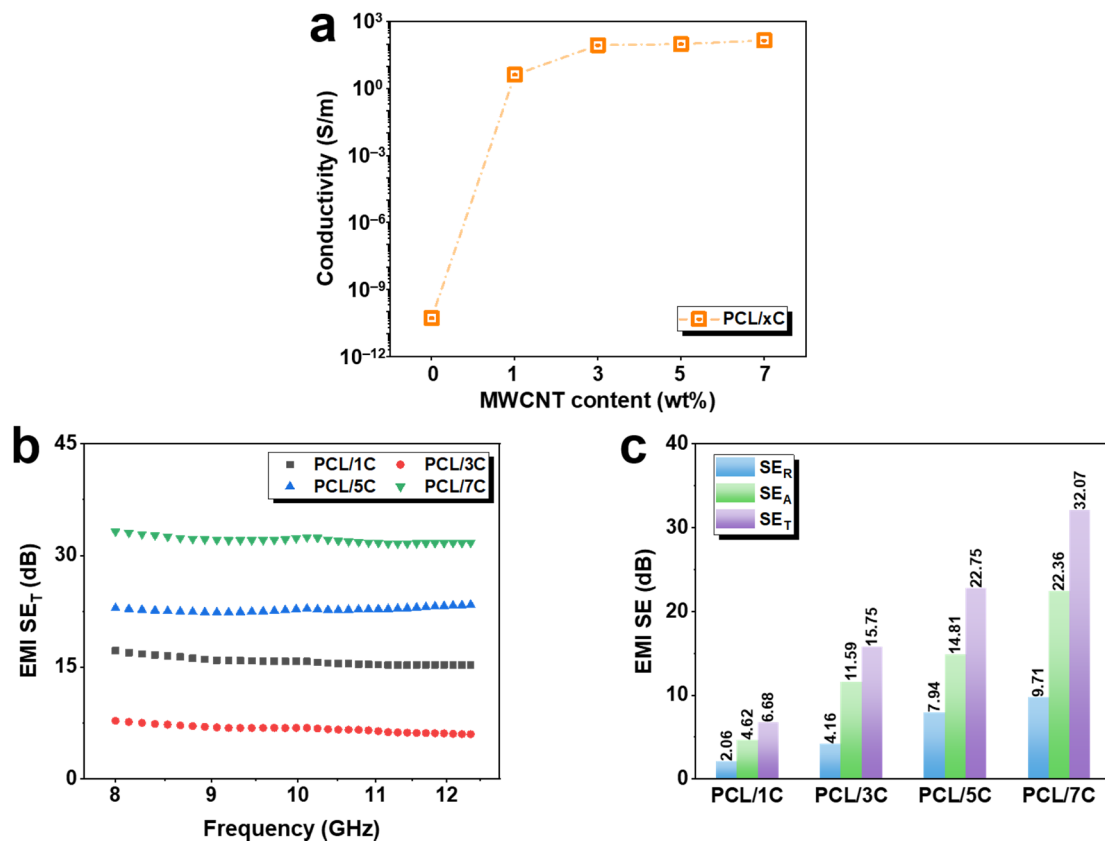

Figure 5. Electrical conductivity and EMI shielding performance of PCL/xC composites: (**a**) electrical conductivity, (**b**) EMI SE_T curves, and (**c**) the correspondingly averaged SE_R, SE_A, and SE_T.

Previous studies have reported that the introduction of a second polymer into the polymer/inorganic particle systems, along with tailoring interfacial interactions and system composition, can strategically regulate the distribution of inorganic particles [50]. This manipulation includes selective dispersion within a specific polymer or at the interface of immiscible blends. We thus incorporated PLA, which is also biodegradable, into the PCL/xC composites using melt blending techniques in order to achieve the selective dispersion of MWCNTs within one of the polymers. Figure 6 presents the rheological

properties of the PCL/PLA/*x*C composites. Analogous to the PCL/*x*C composites, the PCL/PLA/*x*C composites also exhibit typical non-Newtonian fluid behavior with obvious shear thinning tendencies. As the MWCNT content increases, the association between the storage modulus (G′), loss modulus (G″), and frequency gradually diminishes, revealing that a filler network has formed inside the PCL/PLA/*x*C composite. Observations from Figure 7 display the influence of MWCNT on the thermal properties of the PCL/PLA/*x*C composites. The addition of MWCNT, attributed to the heterogeneous nucleation effect, yields a slight increase in the melting temperature and crystallinity of both the PCL and PLA components. In comparison to the PCL/PLA blend, the incorporation of MWCNT triggers a minor advancement in the initial decomposition temperature. This effect can be attributed to the presence of an MWCNT network that expedites the heat transfer process.
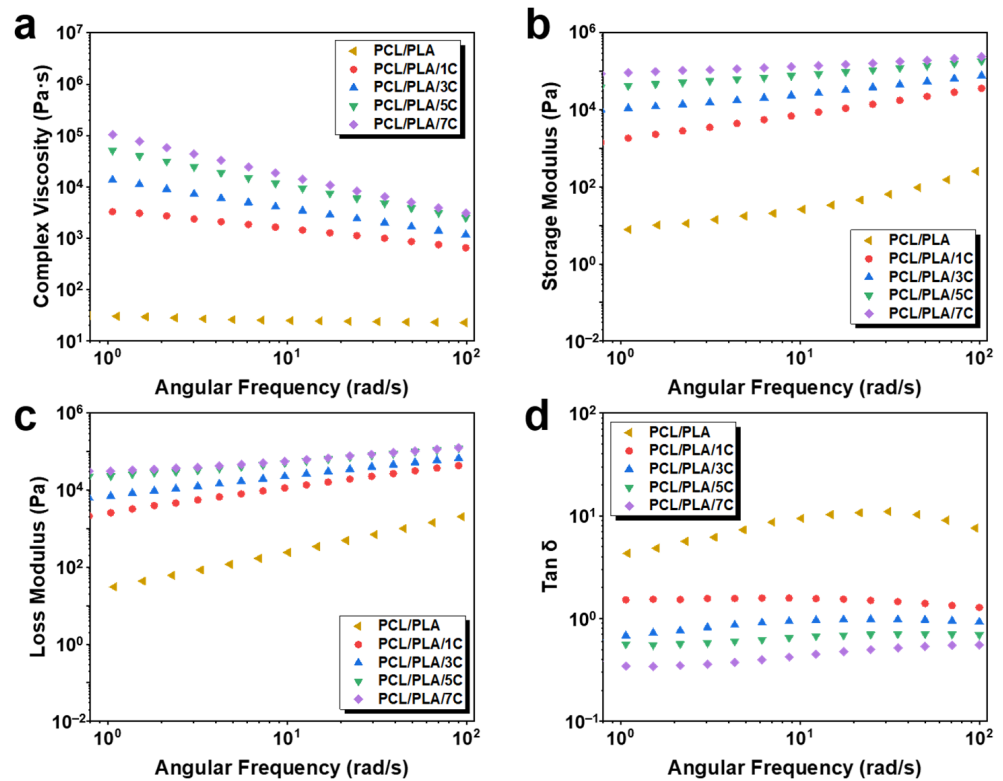

Figure 6. Rheological properties of PCL/PLA/*x*C composites: (**a**) complex viscosity, (**b**) storage modulus, (**c**) loss modulus, and (**d**) tan δ.
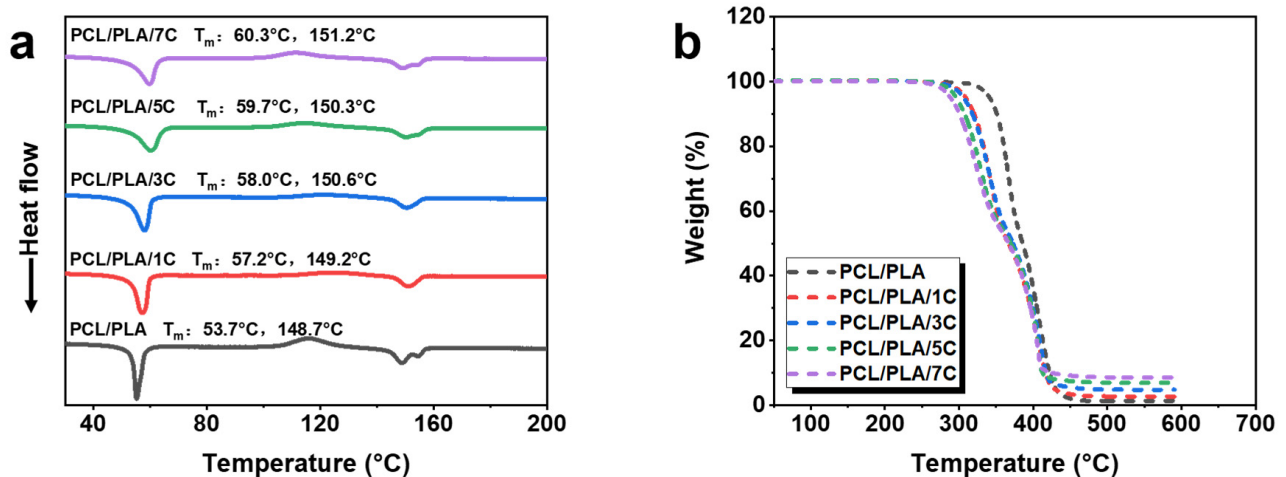

Figure 7. DSC (**a**) and TG (**b**) heating curves of PCL/PLA/*x*C composites.

Figure 8 depicts the cryo-fractured surfaces of the PCL/PLA/*x*C composites, revealing the presence of a typical immiscible system between the PCL and PLA components. In comparison to the PCL/PLA blend (Figure S1b), the introduction of MWCNT brings about a significant reduction in the phase scale, with the domain size inversely correlated with the MWCNT content. This phenomenon is mainly due to the substantial viscosity contrast between PCL and PLA under the same processing temperature and shear field. As mentioned in the Section 2, the preparation of PCL/PLA/*x*C composites is obtained via melt mixing at 180 °C. Given the considerably lower viscosity of the PCL melt in comparison to the PLA melt, the resulting phase domain scale within the PCL/PLA composites tends to be larger. Indeed, the phase morphology of the polymer blends is markedly influenced by the viscosity ratio of each constituent component within specific temperature and shear fields. Interestingly, upon the introduction of MWCNT into the PCL/PLA system, the phase domain scale undergoes a rapid reduction. This behavior is likely attributed to the viscosification effect of MWCNT on the low-viscosity PCL components [51,52]. Notably, from Figure 8, it becomes apparent that regardless of the quantity of added MWCNTs, selective dispersion within one of the polymers prevails (as evidenced by the smooth cross section of the other polymer component). To gain a more detailed insight into the evolution of phase morphology, the PCL/PLA/*x*C composites were treated with glacial acetic acid to remove the PCL component. As shown in Figure 9, all composites (PCL and PLA with equal mass ratio) show a co-continuous structure. MWCNT was conspicuously absent at both the cross section of PLA and the interfaces of the two phases, substantiating the anticipated selective dispersion of MWCNTs within the PCL phase. This is consistent with the existing research conclusions of Tao et al. [53]. Additionally, the phase domain scale experiences a significant reduction with the increase in the MWCNT content, which corresponds well with the observations in Figure 8. Thus, the evolving phase domain scale can be attributed to the progressive increase in viscosity within the PCL/CNT component due to the selective dispersion of MWCNT. Under a consistent temperature and shear environment, the rheological properties of the PLA components remain unaltered, while the PCL/CNT components drive the transformation of the phase domain scale.
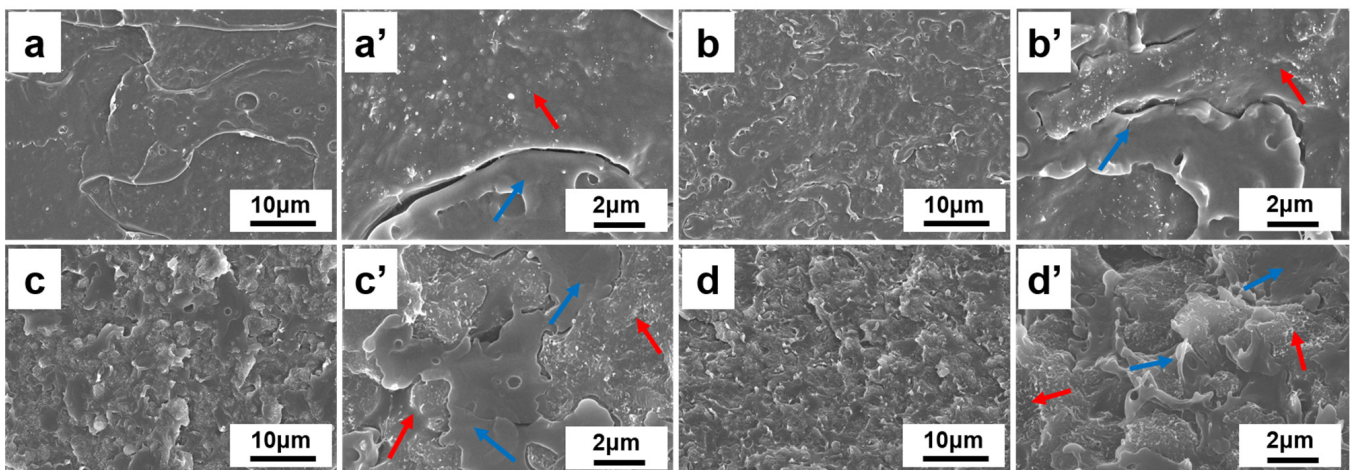

Figure 8. SEM images of cryo-fractured surfaces of PCL/PLA/*x*C composites: (**a**,**a'**) PCL/PLA/1C, (**b**,**b'**) PCL/PLA/3C, (**c**,**c'**) PCL/PLA/5C, and (**d**,**d'**) PCL/PLA/7C. The red arrow represents the PCL phase region and the blue arrow represents the PLA phase region.

Figure 10 presents the electrical conductivity and EMI shielding properties of the PCL/PLA/*x*C composites. As evident in Figure 10a, the addition of MWCNT induces a remarkable improvement in the conductivity of the PCL/PLA/*x*C composites, which is attributed to the successful establishment of a continuous MWCNT network [47]. Furthermore, the electrical conductivity of the PCL/PLA/*x*C composites surpasses that of the PCL/*x*C composites containing the same quantity of MWCNT. Within the PCL/PLA/*x*C

composites, MWCNT is preferentially dispersed within the PCL phase, which means that the concentration of MWCNT in the PCL/MWCNT component of the PCL/PLA/xC composites is significantly higher than that of the PCL/xC composites. The improved MWCNT concentration directly increases the contact probability of single MWCNT in the PCL matrix, thereby facilitating the formation of a dense and robust conducive network. Simultaneously, the PLA component contributes to volume occupation while engaging in a co-continuous structure with the PCL/xC component. This not only reinforces the strength and modulus of the resultant composites, but also capitalizes on these advantageous structural features. Benefiting from these structural enhancements, the total EMI SE of the PCL/PLA/xC composites exhibits a substantial improvement when compared to the PCL/xC composites with the same filler content. Once the MWCNT content exceeds 3 wt%, a satisfactory total EMI SE is achieved, satisfying the essential criteria for commercial applications. Notably, at an MWCNT content of 7 wt%, the SE_T value of the PCL/PLA/7C composite impressively reaches 39.06 dB. However, it is pertinent to highlight that the SE_A/SE_T values of both PCL/PLA/xC and PCL/xC are relatively low. In order to obtain the EMI shielding materials dominated by absorption loss, the optimization and material structure resign are imperative to enhance the SE_A/SE_T ratio [44,54].
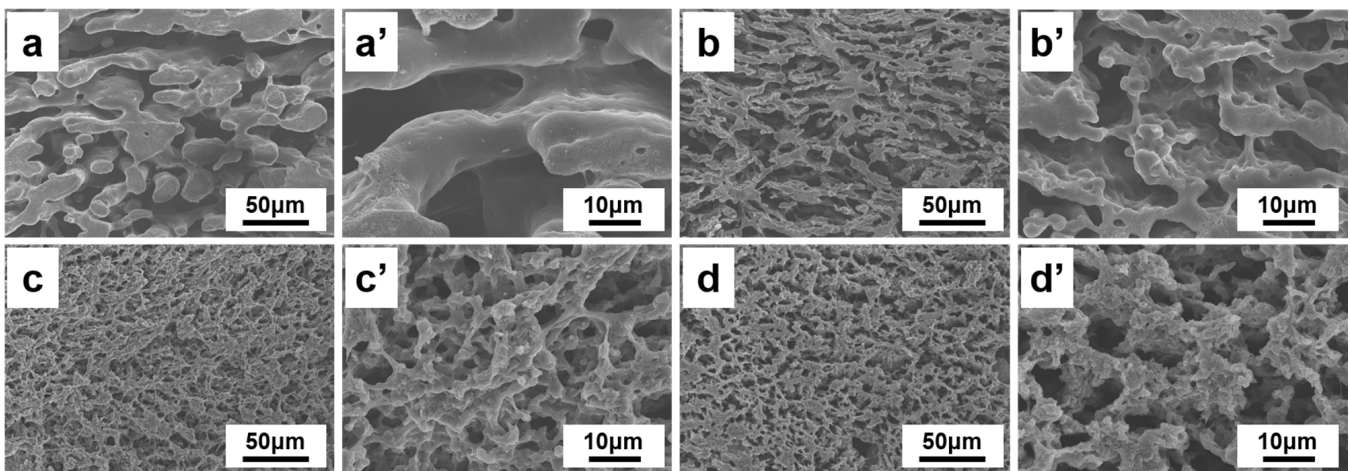

Figure 9. SEM images of PLA phase morphology after removing the PCL region using glacial acetic acid: (**a**,**a'**) PCL/PLA/1C, (**b**,**b'**) PCL/PLA/3C, (**c**,**c'**) PCL/PLA/5C, and (**d**,**d'**) PCL/PLA/7C.

Our previous works demonstrated that suitable porous structures within composites using an accessible strategy could result in a scenario where the EMW is subjected to repeated multiple reflections between pore walls, ultimately being absorbed. Therefore, we undertook the fabrication of porous f-PCL/PLA/xC by initially melt mixing the obtained PCL/PLA/xC composites with NaCl particles, followed by the removal of the pore-inducing agent. Figure 11 displays the observed porous structure via SEM, revealing the complete elimination of NaCl particles and the emergence of uniform porous structures. Notably, the advantages of using NaCl as a pore-inducing agent include a low cost, recyclable reuse, ease of processing, and suitability for large-scale preparation. Moreover, this method offers an enhanced control over structural parameters such as the pore size and porosity compared to alternative approaches [55]. The EMI shielding performance of the f-PCL/PLA/xC samples is shown in Figure 12. While the EMI SE_T value of porous f-PCL/PLA/xC is slightly below that of their solid PCL/PLA/xC counterparts, the SE_T of the f-PCL/PLA/7C sample remains at 22.88 dB, which meets the commercial standards. Notably, in Figure 12b, the SE_A value in the f-PCL/PLA/xC samples significantly surpasses the SE_R value, indicating the predominant role of absorption loss in these porous shielding materials.
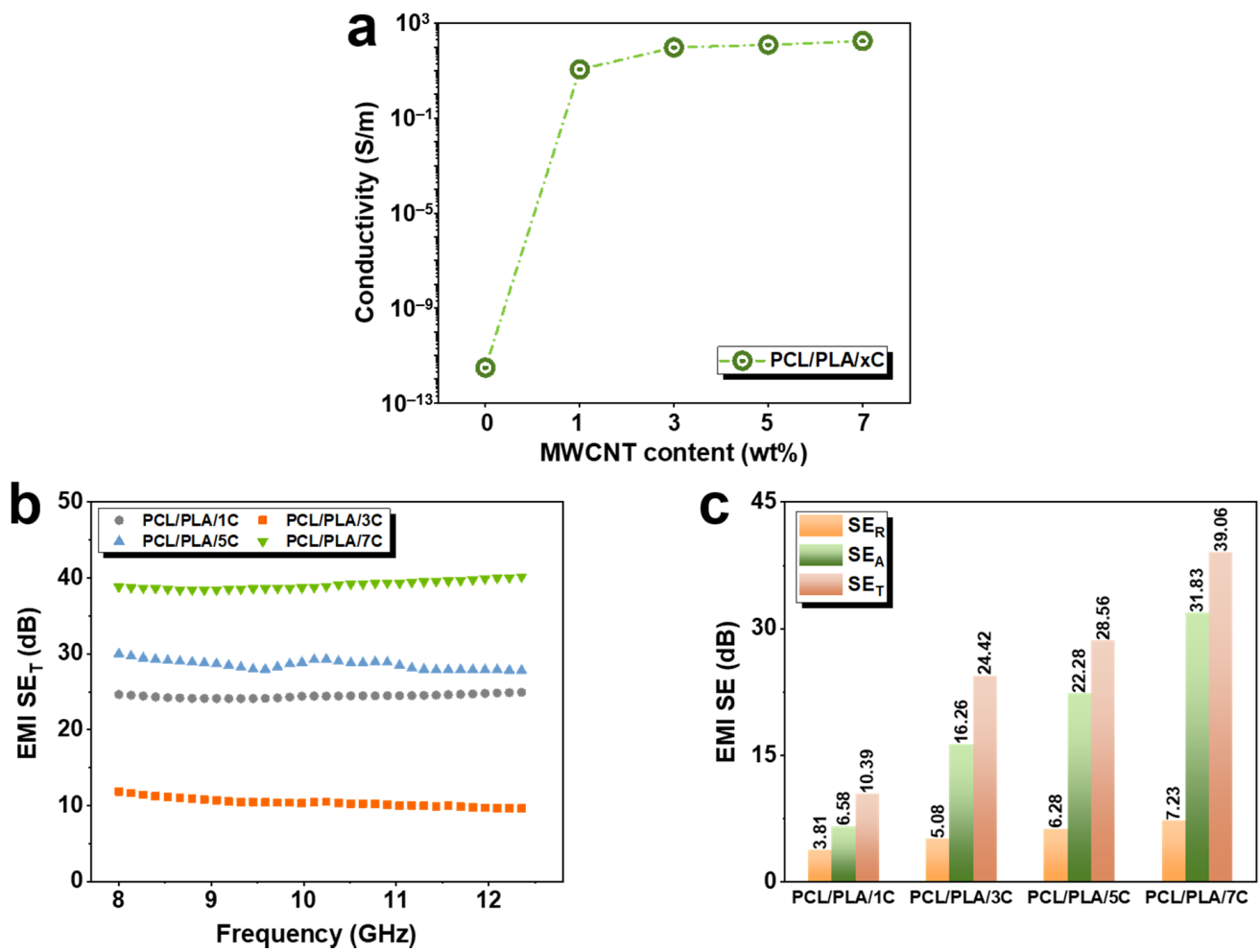
Figure 10. Electrical conductivity and EMI shielding performance of PCL/PLA/*x*C composites: (**a**) electrical conductivity, (**b**) EMI SE_T curves, and (**c**) the correspondingly averaged SE_R, SE_A, and SE_T.
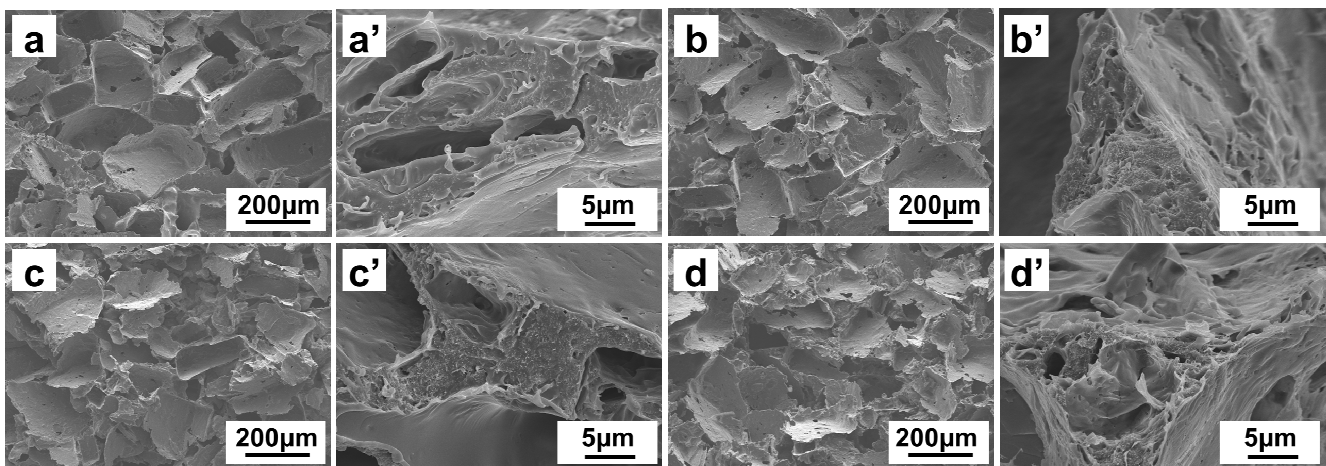

Figure 11. SEM images of cryo-fractured surfaces: (**a**,**a'**) f-PCL/PLA/1C, (**b**,**b'**) f-PCL/PLA/3C, (**c**,**c'**) f-PCL/PLA/5C, and (**d**,**d'**) f-PCL/PLA/7C.
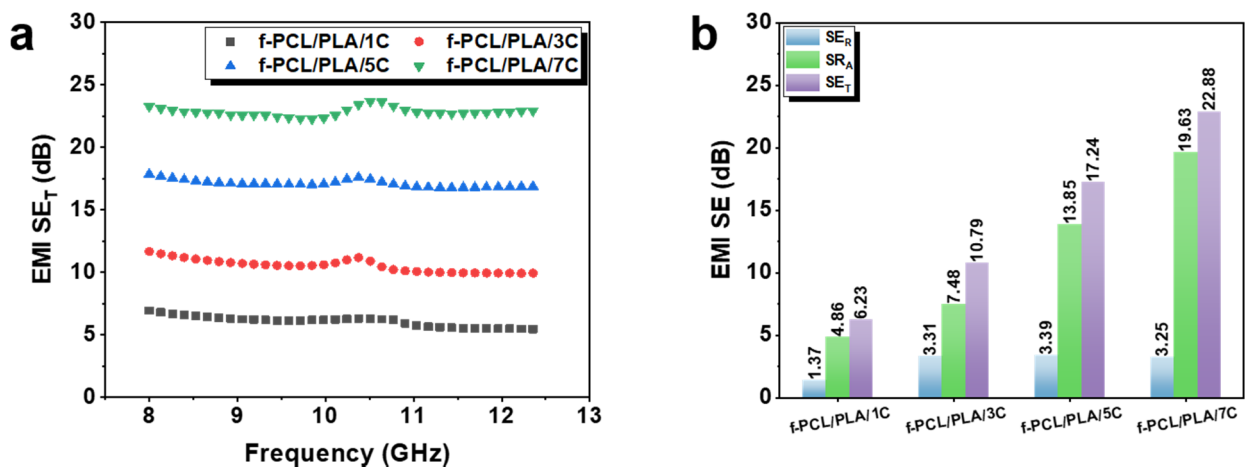
Figure 12. EMI shielding performance of various f-PCL/PLA/xC samples: (**a**) EMI SE_T curves and (**b**) the correspondingly averaged SE_R, SE_A, and SE_T.

To illustrate the influence of the porous structure more obviously on the EMI shielding performance, we calculated the SE_A/SE_T ratio and specific EMI SE_T values for f-PCL/PLA/xC foams and PCL/PLA/xC composites, respectively (as depicted in Figure 13).
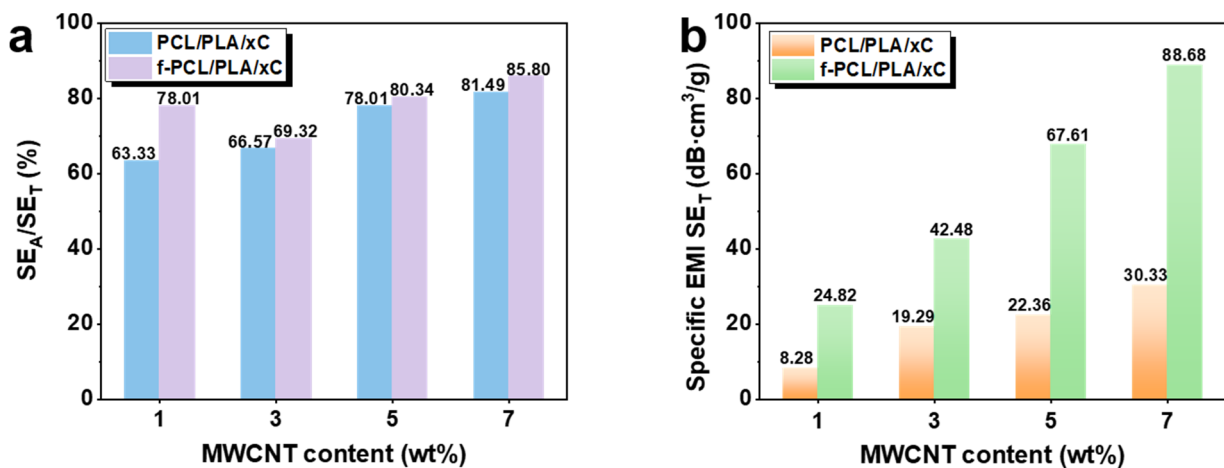

Figure 13. Comparison of EMI shielding performance of PCL/PLA/xC and f-PCL/PLA/xC: (**a**) SE_A/SE_T and (**b**) the calculated thickness-averaged specific EMI SE_T.

Figure 13a shows the difference between the SE_A/SE_T value of the two materials. Owing to the porous structure, the SE_A/SE_T value of the f-PCL/PLA/xC foams is always higher than that of the PCL/PLA/xC composites. However, due to the presence of co-continuous structures in the PCL/PLA/xC composites, its own SE_A/SE_T value is relatively high, so the absorption ratio of electromagnetic waves only has a small increase [8]. Notably, due to the density differential (f-PCL/PLA/xC being merely 20% of the solid PCL/PLA/xC), the latter exhibits a lower SE_T value. Furthermore, Figure 13b highlights the substantial enhancement in the specific EMI SE_T for the f-PCL/PLA/xC foams compared to the PCL/PLA/xC composites. For instance, the specific EMI SE_T of f-PCL/PLA/7C reaches as high as 88.68 dB/(g/cm^3), which is about 2.92 times that of the PCL/PLA/xC composites (30.33 dB/(g/cm^3)). In summary, the f-PCL/PLA/xC foams developed in this study not only exhibit high specific EMI SE_T, but also showcase absorption-dominated characteristics.

Finally, we further investigated the influence of MWCNT on the compressive properties of porous f-PCL/PLA/xC samples. From Figure 14 and Table S2, it can be observed that all f-PCL/PLA/xC foams exhibit a stable and consistent compression performance. The compressive yield strength and compressive modulus are positively correlated with

the MWCNT content, attributing to the strengthening of MWCNT on the polymer matrix. When the MWCNT content increases from 1 wt% to 7 wt%, the compressive yield strength and compressive modulus increase by 76.9% and 226.4%, respectively. Although the rigid MWCNT has a certain strengthening effect on the polymer, the compressive yield strength of all samples is low due to the porosity of the composite foam up to 80%. Additionally, while the rigid MWCNT filler contributes to the reinforcement of the f-PCL/PLA/*x*C samples, it is worth noting that the presence of PLA also plays a strengthening role in this study. As a result, the impact of MWCNT becomes attenuated and less pronounced. Considering the porous characteristics of lightweight f-PCL/PLA/*x*C foams, its stable compression resistance can still meet the basic requirements of many practical applications.
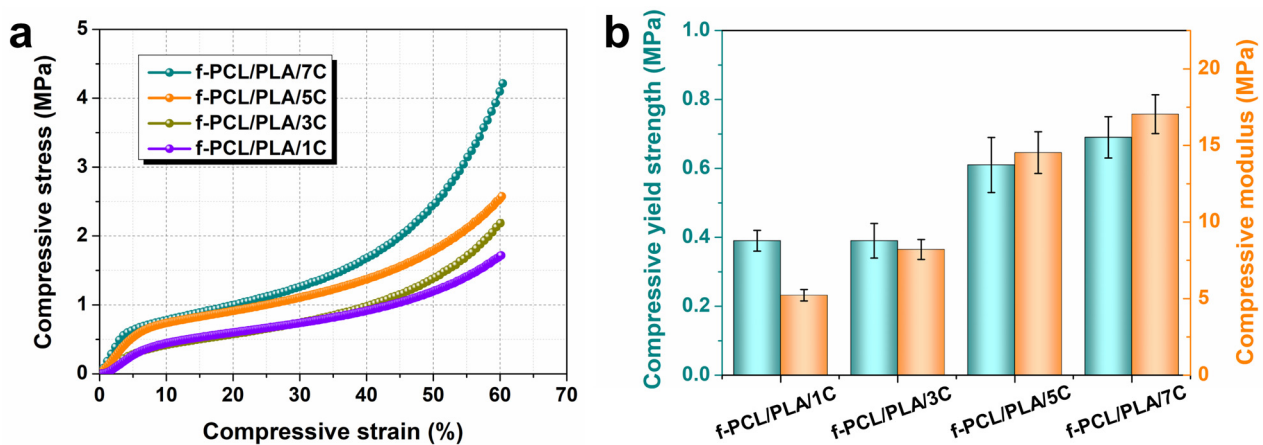

Figure 14. Compressive properties of various f-PCL/PLA/*x*C samples: (**a**) stress–strain curves and (**b**) compressive yield strength and compressive modulus.

4. Conclusions

In summary, we developed an effective, facile, and scalable strategy to fabricate light-weight, absorption-dominated, and biodegradable PCL/PLA/MWCNT composite foams for high-performance EMI shielding by combining melt mixing and particle leaching processes. The MWCNT content exhibits a significant influence on the phase morphology evolution, electrical conductivity, and EMI shielding efficiency. Compared with the PCL/*x*C binary composites, the PCL/PLA/*x*C ternary composites have higher conductivity and EMI shielding performance. This can be attributed to the formation of a co-continuous structure in the PCL/PLA/*x*C ternary composites, and more importantly, the MWCNTs are preferentially distributed in the PCL matrix, which greatly promotes the construction of a robust conductive network. In the case of a 7 wt% MWCNT content, PCL/PLA/7C shows good conductivity and EMI SE_T, up to 179.49 S/m and 39.06 dB, respectively. Moreover, the introduced porous structure further increases the SE_A/SE_T of the sample compared with that of the solid sample, that is, the dominance of absorption loss is more prominent. Optimally, the specific SE_T and SE_A/SE_T of the f-PCL/PLA/7C sample achieve 88.68 dB·cm^3/g and 85.80%, respectively, which are better than 30.33 dB·cm^3/g and 81.49% of the PCL/PLA/7C sample. Thus, the aforementioned conclusions of this work can provide a practical method and unique ideas for the structural design and fabrication of light-weight, absorption-dominated, superior EMI shielding performance and biodegradable polymer-based composite foams, and further widens their application in electronics, aerospace, automotive industries, and wearable intelligent electronic devices.

References

1. Liang, C.; Gu, Z.; Zhang, Y.; Ma, Z.; Qiu, H.; Gu, J. Structural design strategies of polymer matrix composites for electromagnetic interference shielding: A review. *Nano-Micro Lett.* **2021**, *13*, 181. [CrossRef]
2. Ju, J.; Kuang, T.; Ke, X.; Zeng, M.; Chen, Z.; Zhang, S.; Peng, X. Lightweight multifunctional polypropylene/carbon nanotubes/carbon black nanocomposite foams with segregated structure, ultralow percolation threshold and enhanced electromagnetic interference shielding performance. *Compos. Sci. Technol.* **2020**, *193*, 108116. [CrossRef]
3. Wang, M.; Tang, X.-H.; Cai, J.-H.; Wu, H.; Shen, J.-B.; Guo, S.-Y. Construction, mechanism and prospective of conductive polymer composites with multiple interfaces for electromagnetic interference shielding: A review. *Carbon* **2021**, *177*, 377–402. [CrossRef]
4. Zhan, Y.; Santillo, C.; Meng, Y.; Lavorgna, M. Recent advances and perspectives on silver-based polymer composites for electromagnetic interference shielding. *J. Mater. Chem. C* **2023**, *11*, 859–892. [CrossRef]
5. Luo, J.; Sun, W.; Zhou, H.; Zhang, Y.; Wen, B.; Xin, C. Bioderived and biodegradable poly (3-hydroxybutyrate-co-3-hydroxyvalerate) nanocomposites based on carbon nanotubes: Microstructure observation and EMI shielding property improvement. *ACS Sustain. Chem. Eng.* **2021**, *9*, 10785–10798. [CrossRef]
6. Yang, J.; Chen, Y.; Yan, X.; Liao, X.; Wang, H.; Liu, C.; Wu, H.; Zhou, Y.; Gao, H.; Xia, Y. Construction of in-situ grid conductor skeleton and magnet core in biodegradable poly (butyleneadipate-co-terephthalate) for efficient electromagnetic interference shielding and low reflection. *Compos. Sci. Technol.* **2023**, *240*, 110093. [CrossRef]
7. Luo, J.; Zhu, M.; Wang, L.; Zhou, H.; Wen, B.; Wang, X.; Zhang, Y. CO_2-based fabrication of biobased and biodegradable poly (3-hydroxybutyrate-co-3-hydroxyvalerate)/graphene nanoplates nanocomposite foams: Toward EMI shielding application. *Polymer* **2022**, *253*, 125034. [CrossRef]
8. Xu, P.; Huang, B.; Tang, R.; Wang, Z.; Tu, J.; Ding, Y. Improved mechanical and EMI shielding properties of PLA/PCL composites by controlling distribution of PIL-modified CNTs. *Adv. Compos. Hybrid Mater.* **2022**, *5*, 991–1002. [CrossRef]
9. Wang, Y.; Wang, P.; Du, Z.; Liu, C.; Shen, C.; Wang, Y. Electromagnetic interference shielding enhancement of poly (lactic acid)-based carbonaceous nanocomposites by poly (ethylene oxide)-assisted segregated structure: A comparative study of carbon nanotubes and graphene nanoplatelets. *Adv. Compos. Hybrid Mater.* **2022**, *5*, 209–219. [CrossRef]
10. Tao, J.-R.; Tang, X.-H.; He, Q.-M.; Wang, M. Effect of surface conductivity on electromagnetic shielding of multi-walled carbon nanotubes/Poly (ε-caprolactone) composites. *Compos. Sci. Technol.* **2022**, *229*, 109715. [CrossRef]
11. Kashi, S.; Gupta, R.K.; Bhattacharya, S.N.; Varley, R.J. Experimental and simulation study of effect of thickness on performance of (butylene adipate-co-terephthalate) and poly lactide nanocomposites incorporated with graphene as stand-alone electromagnetic interference shielding and metal-backed microwave absorbers. *Compos. Sci. Technol.* **2020**, *195*, 108186.
12. Tian, G.; He, H.; Xu, M.; Liu, Y.; Gao, Q.; Zhu, Z. Ultralow percolation threshold biodegradable PLA/PBS/MWCNTs with segregated conductive networks for high-performance electromagnetic interference shielding applications. *J. Appl. Polym. Sci.* **2023**, *140*, e53558. [CrossRef]
13. Huang, B.; Wang, Z.; Tu, J.; Liu, C.; Xu, P.; Ding, Y. Interfacial distribution and compatibilization of imidazolium functionalized CNTs in poly (lactic acid)/polycaprolactone composites with excellent EMI shielding and mechanical properties. *Int. J. Biol. Macromol.* **2023**, *227*, 1182–1190. [CrossRef] [PubMed]
14. Hou, M.; Feng, Y.; Yang, S.; Wang, J. Multi-hierarchically Structural Polycaprolactone Composites with Tunable Electromagnetic Gradients for Absorption-Dominated Electromagnetic Interference Shielding. *Langmuir* **2023**, *39*, 6038–6050. [CrossRef]
15. Tao, J.-R.; Luo, C.-L.; Huang, M.-L.; Weng, Y.-X.; Wang, M. Construction of unique conductive networks in carbon nanotubes/polymer composites via poly (ε-caprolactone) inducing partial aggregation of carbon nanotubes for microwave shielding enhancement. *Compos. Part A Appl. Sci. Manuf.* **2023**, *164*, 107304. [CrossRef]
16. Wu, B.; Zhu, H.; Yang, Y.; Huang, J.; Liu, T.; Kuang, T.; Jiang, S.; Hejna, A.; Liu, K. Effect of different proportions of $CNTs/Fe_3O_4$ hybrid filler on the morphological, electrical and electromagnetic interference shielding properties of poly (lactic acid) nanocomposites. *e-Polymers* **2023**, *23*, 20230006. [CrossRef]
17. Álvarez, M.; Santos, X.; Fest, A.; Sánchez, D.E.; Baselga, J.; Pozuelo, J. Lightweight Nanostructures of Cellulose Nanofibers and $Ti_3C_2T_x$ MXenes for Their Application in Electromagnetic Interference Shielding. *ACS Appl. Eng. Mater.* **2023**, *1*, 1881–1891. [CrossRef]

18. Yan, K.; Wu, C.; Xie, L.; Zeng, L.; Jiang, Y.; Jiang, Z.; Chang, G.; Xue, B.; Zheng, Q. High EMI shielding effectiveness and superhydrophobic properties based on step-wise asymmetric structure constructed by one-step method. *Nano Res.* **2023**, *16*, 10483–10492. [CrossRef]

19. Yang, J.; Chen, Y.; Liu, C.; Wang, H.; Yan, X.; Chai, X.; Chen, Z.; Xia, Y.; Gao, H.; Zhang, H. Constructing 3D expanded graphite-silver segregated network structure for ultra-efficient EMI shielding and low reflection. *J. Mater. Res. Technol.* **2023**, *23*, 5115–5126. [CrossRef]

20. Li, J.; Zhang, W.; Yang, L.; Yin, S. Conductive fabrics based on carbon nanotube/Ti$_3$C$_2$T$_x$ MXene/polyaniline/liquid metal quaternary composites with improved performance of EMI shielding and joule heating. *Compos. Commun.* **2023**, *38*, 101476. [CrossRef]

21. Yao, Y.; Jin, S.; Wang, M.; Gao, F.; Xu, B.; Lv, X.; Shu, Q. MXene hybrid polyvinyl alcohol flexible composite films for electromagnetic interference shielding. *Appl. Surf. Sci.* **2022**, *578*, 152007. [CrossRef]

22. Tan, Z.; Zhao, H.; Sun, F.; Ran, L.; Yi, L.; Zhao, L.; Wu, J. Fabrication of Chitosan/MXene multilayered film based on layer-by-layer assembly: Toward enhanced electromagnetic interference shielding and thermal management capacity. *Compos. Part A Appl. Sci. Manuf.* **2022**, *155*, 106809. [CrossRef]

23. Yang, S.; Wang, Y.-Y.; Song, Y.-N.; Jia, L.-C.; Zhong, G.-J.; Xu, L.; Yan, D.-X.; Lei, J.; Li, Z.-M. Ultrathin, flexible and sandwich-structured PHBV/silver nanowire films for high-efficiency electromagnetic interference shielding. *J. Mater. Chem. C* **2021**, *9*, 3307–3315. [CrossRef]

24. Kim, J.; Kim, G.; Kim, S.-Y.; Lee, S.; Kim, Y.; Lee, J.; Kim, J.; Jung, Y.C.; Kwon, J.; Han, H. Fabrication of highly flexible electromagnetic interference shielding polyimide carbon black composite using hot-pressing method. *Compos. Part B Eng.* **2021**, *221*, 109010. [CrossRef]

25. Zhang, C.; Lv, Q.; Liu, Y.; Wang, C.; Wang, Q.; Wei, H.; Liu, L.; Li, J.; Dong, H. Rational design and fabrication of lightweight porous polyimide composites containing polyaniline modified graphene oxide and multiwalled carbon nanotube hybrid fillers for heat-resistant electromagnetic interference shielding. *Polymer* **2021**, *224*, 123742. [CrossRef]

26. Xu, Z.; Zhang, Y.; Wang, Z.; Sun, N.; Li, H. Enhancement of electrical conductivity by changing phase morphology for composites consisting of polylactide and poly (ε-caprolactone) filled with acid-oxidized multiwalled carbon nanotubes. *ACS Appl. Mater. Interfaces* **2011**, *3*, 4858–4864. [CrossRef] [PubMed]

27. Liu, Z.; Bai, H.; Luo, Y.; Zhang, Q.; Fu, Q. Achieving a low electrical percolation threshold and superior mechanical performance in poly (l-lactide)/thermoplastic polyurethane/carbon nanotubes composites via tailoring phase morphology with the aid of stereocomplex crystallites. *RSC Adv.* **2017**, *7*, 11076–11084. [CrossRef]

28. Chen, J.; Cui, X.; Zhu, Y.; Jiang, W.; Sui, K. Design of superior conductive polymer composite with precisely controlling carbon nanotubes at the interface of a co-continuous polymer blend via a balance of π-π interactions and dipole-dipole interactions. *Carbon* **2017**, *114*, 441–448. [CrossRef]

29. Chen, J.; Du, X.-C.; Zhang, W.-B.; Yang, J.-H.; Zhang, N.; Huang, T.; Wang, Y. Synergistic effect of carbon nanotubes and carbon black on electrical conductivity of PA6/ABS blend. *Compos. Sci. Technol.* **2013**, *81*, 1–8. [CrossRef]

30. Chen, J.; Shen, Y.; Yang, J.-h.; Zhang, N.; Huang, T.; Wang, Y.; Zhou, Z.-w. Trapping carbon nanotubes at the interface of a polymer blend through adding graphene oxide: A facile strategy to reduce electrical resistivity. *J. Mater. Chem. C* **2013**, *1*, 7808–7811. [CrossRef]

31. Ma, L.; Hamidinejad, M.; Wei, L.; Zhao, B.; Park, C.B. Absorption-dominant EMI shielding polymer composite foams: Microstructure and geometry optimization. *Mater. Today Phys.* **2023**, *30*, 100940. [CrossRef]

32. Park, C.B.; Ma, L.; Hamidinejad, M.; Wei, L. Layered Polymer Composite Foams for Broadband Ultra-Low Reflectance EMI Shielding: A Computationally Guided Fabrication Approach. *Mater. Horiz.* **2023**. [CrossRef]

33. Fu, H.; Duan, S.; Zhou, H.; Gong, W. Structure design of multi-layered ABS/CNTs composite foams for EMI shielding application with low reflection and high absorption characteristics. *Appl. Surf. Sci.* **2023**, *624*, 157168. [CrossRef]

34. Wu, Y.; Yu, K.; Zhang, X.; Hou, J.; Chen, J. Lightweight electromagnetic interference shielding poly (L-lactic acid)/poly (D-lactic acid)/carbon nanotubes composite foams prepared by supercritical CO$_2$ foaming. *Int. J. Biol. Macromol.* **2022**, *210*, 11–20. [CrossRef]

35. Kuang, T.; Ju, J.; Chen, F.; Liu, X.; Zhang, S.; Liu, T.; Peng, X. Coupled effect of self-assembled nucleating agent, Ni-CNTs and pressure-driven flow on the electrical, electromagnetic interference shielding and thermal conductive properties of poly (lactic acid) composite foams. *Compos. Sci. Technol.* **2022**, *230*, 109736. [CrossRef]

36. Sushmita, K.; Ghosh, D.; Nilawar, S.; Bose, S. Absorption dominated directional electromagnetic interference shielding through asymmetry in a multilayered construct with an exceptionally high green index. *ACS Appl. Mater. Interfaces* **2022**, *14*, 49140–49157. [CrossRef]

37. Bera, R.; Das, A.K.; Maitra, A.; Paria, S.; Karan, S.K.; Khatua, B.B. Salt leached viable porous Fe$_3$O$_4$ decorated polyaniline–SWCNH/PVDF composite spectacles as an admirable electromagnetic shielding efficiency in extended Ku-band region. *Compos. Part B Eng.* **2017**, *129*, 210–220. [CrossRef]

38. Xu, L.; Jia, L.-C.; Yan, D.-X.; Ren, P.-G.; Xu, J.-Z.; Li, Z.-M. Efficient electromagnetic interference shielding of lightweight carbon nanotube/polyethylene composites via compression molding plus salt-leaching. *RSC Adv.* **2018**, *8*, 8849–8855. [CrossRef]

39. Yang, H.; Yu, Z.; Wu, P.; Zou, H.; Liu, P. Electromagnetic interference shielding effectiveness of microcellular polyimide/in situ thermally reduced graphene oxide/carbon nanotubes nanocomposites. *Appl. Surf. Sci.* **2018**, *434*, 318–325. [CrossRef]

40. Chen, J.; Wang, Y.; Gu, Z.; Huang, J.; He, W.; Liu, P. Rational design of hierarchical yolk-double shell Fe@ NCNs/MnO$_2$ via thermal-induced phase separation toward wideband microwave absorption. *Carbon* **2023**, *204*, 305–314. [CrossRef]

41. Sang, G.; Xu, P.; Yan, T.; Murugadoss, V.; Naik, N.; Ding, Y.; Guo, Z. Interface engineered microcellular magnetic conductive polyurethane nanocomposite foams for electromagnetic interference shielding. *Nano-Micro Lett.* **2021**, *13*, 1–16. [CrossRef] [PubMed]

42. Zeng, Z.; Jin, H.; Chen, M.; Li, W.; Zhou, L.; Zhang, Z. Lightweight and anisotropic porous MWCNT/WPU composites for ultrahigh performance electromagnetic interference shielding. *Adv. Funct. Mater.* **2016**, *26*, 303–310. [CrossRef]

43. Xiao, H.; Lv, J.-B.; Tan, W.; He, X.; Chen, M.-H.; Zeng, K.; Hu, J.-H.; Yang, G. Ultrasound-assisted freeze-drying process for polyimide aerogels. *Chem. Eng. J.* **2022**, *450*, 138344. [CrossRef]

44. Duan, H.; Zhu, H.; Gao, J.; Yan, D.-X.; Dai, K.; Yang, Y.; Zhao, G.; Liu, Y.; Li, Z.-M. Asymmetric conductive polymer composite foam for absorption dominated ultra-efficient electromagnetic interference shielding with extremely low reflection characteristics. *J. Mater. Chem. A* **2020**, *8*, 9146–9159. [CrossRef]

45. Zhao, B.; Hamidinejad, M.; Wang, S.; Bai, P.; Che, R.; Zhang, R.; Park, C.B. Advances in electromagnetic shielding properties of composite foams. *J. Mater. Chem. A* **2021**, *9*, 8896–8949. [CrossRef]

46. Kuang, T.; Chang, L.; Chen, F.; Sheng, Y.; Fu, D.; Peng, X. Facile preparation of lightweight high-strength biodegradable polymer/multi-walled carbon nanotubes nanocomposite foams for electromagnetic interference shielding. *Carbon* **2016**, *105*, 305–313. [CrossRef]

47. Kuang, T.; Zhang, M.; Chen, F.; Fei, Y.; Yang, J.; Zhong, M.; Wu, B.; Liu, T. Creating poly (lactic acid)/carbon nanotubes/carbon black nanocomposites with high electrical conductivity and good mechanical properties by constructing a segregated double network with a low content of hybrid nanofiller. *Adv. Compos. Hybrid Mater.* **2023**, *6*, 48. [CrossRef]

48. Sanchez-Garcia, M.; Lagaron, J.; Hoa, S. Effect of addition of carbon nanofibers and carbon nanotubes on properties of thermoplastic biopolymers. *Compos. Sci. Technol.* **2010**, *70*, 1095–1105. [CrossRef]

49. Ma, Z.; Li, J.; Zhang, J.; He, A.; Dong, Y.; Tan, G.; Ning, M.; Man, Q.; Liu, X. Ultrathin, flexible, and high-strength Ni/Cu/metallic glass/Cu/Ni composite with alternate magneto-electric structures for electromagnetic shielding. *J. Mater. Sci. Technol.* **2021**, *81*, 43–50. [CrossRef]

50. Qi, X.-D.; Yang, J.-H.; Zhang, N.; Huang, T.; Zhou, Z.-W.; Kühnert, I.; Pötschke, P.; Wang, Y. Selective localization of carbon nanotubes and its effect on the structure and properties of polymer blends. *Prog. Polym. Sci.* **2021**, *123*, 101471. [CrossRef]

51. Vega, J.F.; Fernández-Alcázar, J.; López, J.V.; Michell, R.M.; Pérez-Camargo, R.A.; Ruelle, B.; Martínez-Salazar, J.; Arnal, M.L.; Dubois, P.; Müller, A.J. Competition between supernucleation and plasticization in the crystallization and rheological behavior of PCL/CNT-based nanocomposites and nanohybrids. *J. Polym. Sci. Part B Polym. Phys.* **2017**, *55*, 1310–1325. [CrossRef]

52. Zong, R.; Hu, X.; Shang, M.; Wu, C.; Shentu, B. Phase Morphology and Conductive Properties of PBT/POE-g-GMA/PP/CNT Nanocomposites with a Tri-Continuous Structure via Thermal Annealing. *Ind. Eng. Chem. Res.* **2023**, *62*, 8289–8296. [CrossRef]

53. Tao, J.-R.; Yang, D.; Yang, Y.; He, Q.-M.; Fei, B.; Wang, M. Migration mechanism of carbon nanotubes and matching viscosity-dependent morphology in Co-continuous Poly(lactic acid)/Poly(ε-caprolactone) blend: Towards electromagnetic shielding enhancement. *Polymer* **2022**, *252*, 124963. [CrossRef]

54. Wang, Z.; Wang, S.; Zhang, K.; Shen, Z.; Yu, E.; Zheng, S.; Liu, S.; Yang, J. Heterostructured composite foam with highly efficient absorption-dominant EMI shielding capability and mechanical robustness. *Compos. Commun.* **2023**, *40*, 101603. [CrossRef]

55. Salerno, A.; Zeppetelli, S.; Di Maio, E.; Iannace, S.; Netti, P.A. Processing/structure/property relationship of multiscaled PCL and PCL-HA composite scaffolds prepared via gas foaming and NaCl reverse templating. *Biotechnol. Bioeng.* **2011**, *108*, 963–976. [CrossRef]